J Mater Sci: Mater Electron (2013) 24:2218–2227
DOI 10.1007/s10854-013-1082-9

Analysis of indentation size effect (ISE) behavior in low-load Vickers microhardness testing of $(Sm123)_{1-x}(Nd123)_x$ superconductor system

S. Celik · O. Ozturk · E. Coşkun · M. Sarıhan · E. Asikuzun · K. Ozturk · C. Terzioglu

Received: 13 November 2012 / Accepted: 15 January 2013 / Published online: 23 January 2013

Abstract Indentation size effect (*ISE*) for $(Sm123)_{1-x}(Nd123)_x$ superconducting samples which were fabricated by the solid state reaction technique for values of $x = 0.00$, 0.05, 0.10, 0.20, and 0.30 was investigated by analyzing the theoretical models. When the experimental data of a number of single crystals which have the different crystal structure and different chemical bonding inside the polycrystallined samples were analyzed with the *ISE* models, the sample encountering with resistance and elastic deformation was observed as well as plastic deformation. The microhardness values on different surfaces of materials were calculated by using Meyer Law, proportional specimen resistance model, modified proportional specimen resistance model, elastic/plastic deformation model and the Hays–Kendall (*HK*) approach. The results showed that the *HK* approach was determined as the most successful model. Furthermore, X-ray powder diffraction and scanning electron microscope measurements were analyzed for superconducting properties of $(Sm123)_{1-x}(Nd123)_x$ superconductor system. The results showed that microhardness values at the minimum load and averaged plateau region of load increased with increase of Nd123 concentration. Nd123 content can be used as to be estimated the microhardness value of $(Sm123)_{1-x}(Nd123)_x$ superconducting sample in the range of 0.878–2.717 GPa. The control of the microhardness value by using Nd123 content in $(Sm123)_{1-x}(Nd123)_x$ superconducting structure can be useful in technological applications in superconductivity industry.

S. Celik (✉) · E. Coşkun · M. Sarıhan
Department of Physics, Faculty of Arts and Sciences, Recep Tayyip Erdogan University, 53100 Rize, Turkey
e-mail: sukrucelik@yahoo.com

O. Ozturk · E. Asikuzun
Department of Physics, Faculty of Arts and Sciences, Kastamonu University, 37100 Kastamonu, Turkey

K. Ozturk
Department of Physics, Faculty of Sciences, Karadeniz Teknical University, Trabzon, Turkey

C. Terzioglu
Department of Physics, Faculty of Arts and Sciences, Abant İzzet Baysal University, Bolu, Turkey

1 Introduction

Superconducting properties of high-Tc materials such as critical temperature, critical current density, and critical magnetic field are important for the technological applications. One of the applications is superconducting wire. After the fabrication of the wires, mechanical stress is very important because they are wound to form coils. The bending makes the inner side stressed and the outer side of the wire strained. The strain and stress started from grain boundary of the superconducting wire. These strains and stresses can result in cracks which decrease the critical current density of the wire abruptly. The investigation of the mechanical properties such as the stress of the materials can be done by using the indentation hardness technique. In this technique, the load which is not destructive to the surface because of the small value is applied to the indenter to form an indentation on the surface of the materials. The hardness can be calculated from the size of the indentation on the surface of the material. On the other hand, because the hardness is related to the structure and composition of the material, this technique is used to characterize materials [1]. Three dominant properties of the superconducting materials which are crystal structure, grain orientation and

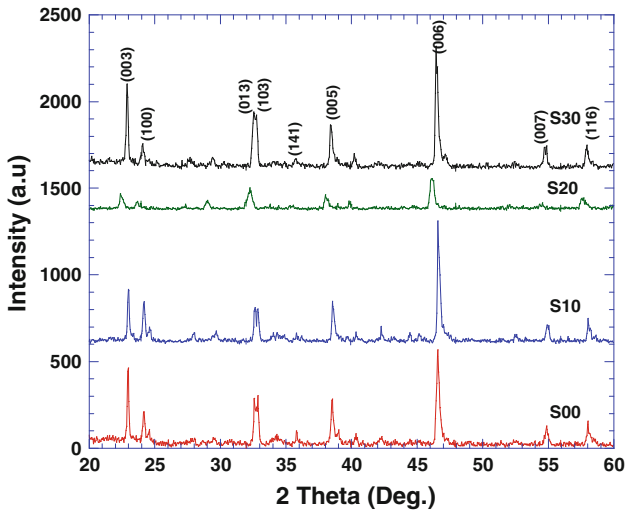

Fig. 1 *XRD* patterns of the *S00*, *S10*, *S20* and *S30* samples

Table 1 Lattice parameters *a, b, c* and grain size results for the samples

Samples	a (Å)	b (Å)	c (Å)	Grain size (nm)
S00	3.705	4.247	11.656	97.04
S10	3.752	4.056	11.675	88.96
S20	3.694	3.974	11.815	41.43
S30	3.643	3.990	11.733	68.47

porosity [2] are effective in indentation. Because the porosity is oppositely proportional to the hardness [3], the results of hardness must be supported by XRD and SEM results.

Hardness can be defined as the resistance of materials against to prick a rigid tip. In this experiment, a standard edge is suppressed on object with a constant load. The size of track is evaluated as a measure of plastic (permanent) deformation resistance of the material. The measured hardness values are only the number of comparison, so measured data are not used from direct in designs. However, this method is a widely used method in the quality control, especially, because it can be conducted easier and it provides information about the behavior of toughness and corrosion of materials. Among the different hardness methods, it is very important to use the most appropriate one for the type and the hardness of a material. Brinell test, Vickers test, Rockwell test are some hardness tests. A square base diamond pyramid with an apex angle of 136° is used for the Vickers microhardness tests used in our study. Loads vary from 10 to 1,200 N. The surface is determined by taking the average of diagonals of the indentation and Vickers microhardness is calculated by load/area of indentation equation. Vickers hardness measurement method can be applied to all materials and it gives very accurate results.

The hardness in the area of the intergrains can be changed by the welding of two grains in the structure. By this way, the material can be made stronger against to the stress. Our goal in this study is that sintered Nd123 powder was added to the calcined Sm123 powder in the molar ratio to start the solidification of Sm123 from Nd123 structure in solid form whose decomposition temperature is higher than that of Sm123 in the sintering process of Sm123 to weld Nd123 grains each other. The samples Nd123 and Sm123 samples were fabricated by solid-state-reaction technique. Not only were XRD measurements done to analyze the lattice parameters, but also SEM measurements were performed to examine the surface structure and grain orientation. The results of the measurements were used to analyze the mechanic properties using various models.

2 Experimental details

Nd123 samples, prepared by solid state reaction method in the cylindrical shape, were calcined twice and sintered at the temperatures of 900, 940 and 1,033 °C, respectively. After grinded of Nd123 pellets, the powder mixed at the stoichiometric ratio of x = 0.00, 0.05, 0.10, 0.20 and 0.30 into the calcined Sm123 powder at 940 °C and then sintered at the temperature of 940 °C for 6 h. The sintered samples in cylindrical pellet form were oxygenated at 450 °C for 4 h together. Both heating and cooling rates were adjusted to be 5 and 2 °C/min., respectively. All the thermal processes were performed the same for each content x.

The prepared samples were characterized using X-ray powder diffraction (XRD) using with Bruker D8 Advance XRD device, scanning electron microscope (SEM) with JEOL 6390-LV, and microhardness measurements (H_v) by using Shimadzu HVM-2 model digital microhardness tester. The volume fraction and the lattice parameters were determined from XRD measurements. The microstructure and surface morphology of the samples were estimated from SEM measurements. Mechanical characterization of the samples was determined from the room temperature microhardness measurements, at different loads (0.245–2.940 N) for 10 s. Vickers microhardness results which were calculated by the different models were used to determine the load independent microhardness values of the samples.

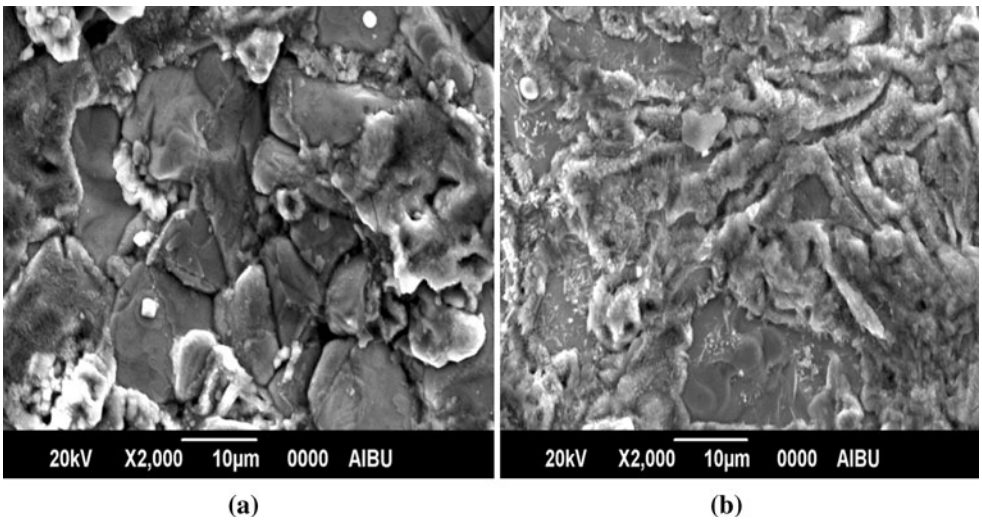

Fig. 2 *SEM* micrographs of **a** *S00* and **b** *S30* samples

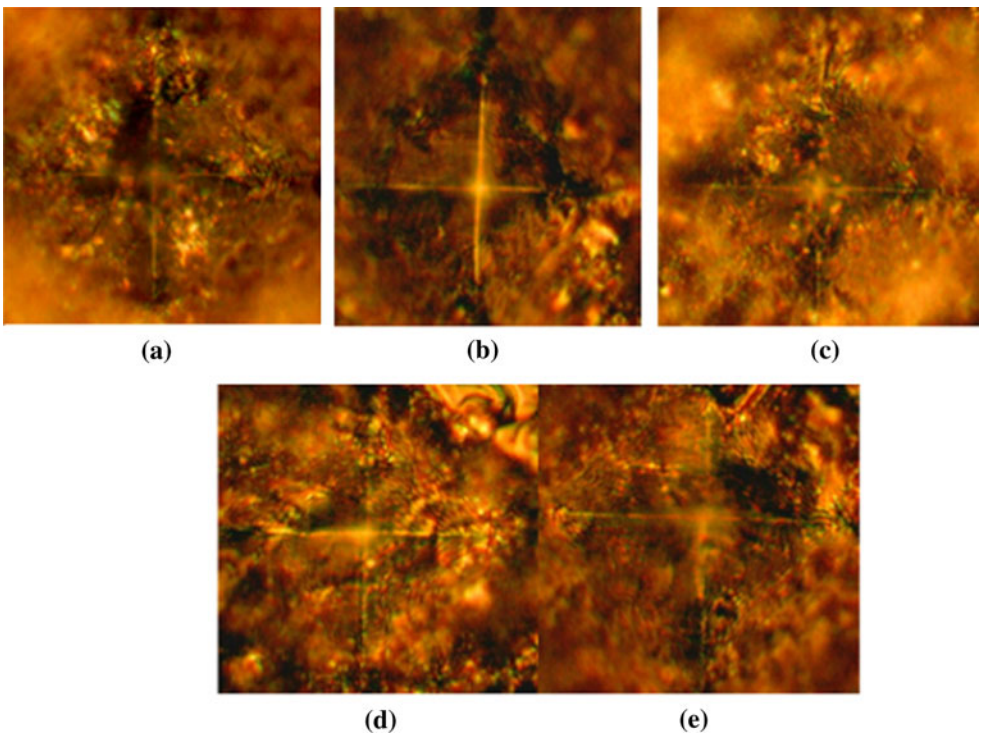

Fig. 3 Optical trace photographs under 2.940 *N* of **a** *S00*, **b** *S05*, **c** *S10*, **d** *S20* and **e** *S30* samples

3 Results and discussion

3.1 XRD Analyses

X-ray diffraction patterns of the prepared samples are shown in Fig. 1. The peaks of (003), (100), (013), (103), (005), (006), (007) and (116) of the 123 structure were seen in spectra of the specimens. Also, (141) peak relating to 211 tetragonal structure that is very low intensity was observed at 35,821° in x = 0.00 undoped sample. Compared with peak intensities of other doped samples at same angle, peak intensities of sample S20 were observed far smaller and also orthorhombic structure was preserved with increasing doping. Lattice parameters were calculated with the least squares method using indices (*h*, *k*, *l*) and the distance between the planes. Lattice parameters *a*, *b*, *c* and *V* (volume) values were

Table 2 The calculated load dependent H_v, E, Y and K_{IC} for the samples

Samples	F (N)	H_v (GPa)	E (GPa)	Y (GPa)	K_{ic} (Pa/m$^{1/2}$)
S00	0.245	1.656	135.73	0.552	1,561.3
	0.490	1.298	106.38	0.432	1,382.2
	0.980	1.100	90.15	0.366	1,272.4
	1.960	0.930	76.22	0.310	1,170.0
	2.940	0.878	71.96	0.292	1,136.8
S05	0.245	2.321	190.23	0.773	1,645.8
	0.490	1.412	115.73	0.470	1,283.7
	0.980	1.184	97.04	0.394	1,175.5
	1.960	1.175	96.30	0.391	1,171.0
	2.940	1.117	91.55	0.372	1,141.7
S10	0.245	3.526	289.00	1.175	2,375.1
	0.490	1.837	150.56	0.612	1,714.3
	0.980	1.766	144.74	0.588	1,680.8
	1.960	1.755	143.84	0.585	1,675.6
	2.940	1.670	136.87	0.556	1,634.5
S20	0.245	3.810	312.28	1.270	2,707.8
	0.490	2.290	187.69	0.763	2,099.2
	0.980	2.235	183.18	0.745	2,073.9
	1.960	1.902	155.89	0.634	1,913.1
	2.940	1.887	154.66	0.629	1,905.6
S30	0.245	3.823	313.34	1.274	2,153.4
	0.490	2.804	229.82	0.934	1,844.2
	0.980	2.717	222.69	0.905	1,815.4
	1.960	2.600	213.10	0.866	1,775.9
	2.940	2.550	209.00	0.850	1,758.7

listed in Table 1. It's clear that the volume of the unit cell decreases with increase of Nd123 content. While Sm123 structure is decreasing with increasing x, Nd123 structure increases. During the sintering process, Sm123 structure is liquid and Nd123 structure is solid state near the melting temperature.

Solidification of molten form structure of Sm123 can start from Nd123 solid structure. Therefore, lattice parameters of Sm123 are expected to be close to lattice parameters of Nd123. c lattice parameters of the Sm123 and Nd123 are 11,709 Å [4] and 11.74 Å, respectively. Parameter c was calculated as 11,656 Å for $x = 0.00$ as listed in Table 1, lattice parameters of a and b decrease linearly with increasing doping and c parameter is almost same for the samples of x = 0.00 and 0.10. That parameter is near the value of Nd123 for the sample x = 0.30. the parameter for the sample x = 0.20 is higher than Nd123 structure. When the intensities and FWHM values of XRD pattern of the sample x = 0.20 is examined, it is clear that the value of parameter c has large error range. So, this means that that value is thought to be near the value of Nd123 structure. Also, volume decreases as linearly with increasing doping.

When to compare XRD pattern of the sample S20 with that of the other samples, the (006) peak intensities of the samples S00, S10, S20 and S30 are 568, 712, 180 and 718, respectively. The intensity of S10 is higher than that of S00 although the amount of Sm123 decreased. The solidification of Sm123 started from the solid Nd123 parts and resulted in increase the number of the crystals and decreased the grain size in the structure. This means that Sm123 structure is dominant in the samples S00 and S10. As for the sample S20, the dominant structures are not only Sm123 but also Nd123. The number of solidification centers increased and resulted in decrease the grain size. There are small crystals of Nd123 and Sm123 in the sample S20. This can be understood from FWHM of the peaks in the XRD spectrum of the sample S20 in Fig. 1. On the other hand, the peak intensities of XRD spectrum of the sample S30 are higher than that of S20. In this sample, beside Nd123 structure is dominant because it is in solid form in sintering process; the number of solidification center is higher than that of S20 and result in smaller grain size of Sm123. So, the peak intensities of S30 are thought to belong to not only Sm123 but also Nd123 structures. This means that large number of small grain sized Sm123 crystal grains and Nd123 grains increased the peak intensities in XRD pattern of this sample. Because of the intensities and the parameter c value, dominant structure is Nd123 in the sample x = 0.30 (S30), and resulted in the lattice parameter to be same as that of Nd123.

3.2 SEM Analyses

The surface morphology, Nd123 doping accumulation in the grain boundaries and orientations of the grains of the $(Sm123)_{1-x}(Nd123)_x$ system were investigated by SEM. Figure 2 shows the surface structure of S00 and S30 samples. It's clear that surface morphology of the samples changes with the increasing of x from 0.00 to 0.30. Grain size and orientations of the samples reduce with increase x. The decrease in grain sizes is also confirmed by the grain size calculations by Scherrer–Warren methods using XRD peaks. As a result, porosity decreases with increase x, the grain approach to another one and grain connectivity enhances.

3.3 Grain size calculation

The grain sizes of the samples were calculated from the XRD patterns measured by X-ray diffractometer by using the following equation (Scherrer–Warren equation)

$$D = \frac{(0.941\lambda)}{(\beta\cos\theta_\beta)} \quad (1)$$

where D is grain size (nm), λ is the wave length of X-ray (0.154 nm), β is the FWHM of the highest intensity peak and θ is the corresponding angle of the peak. The

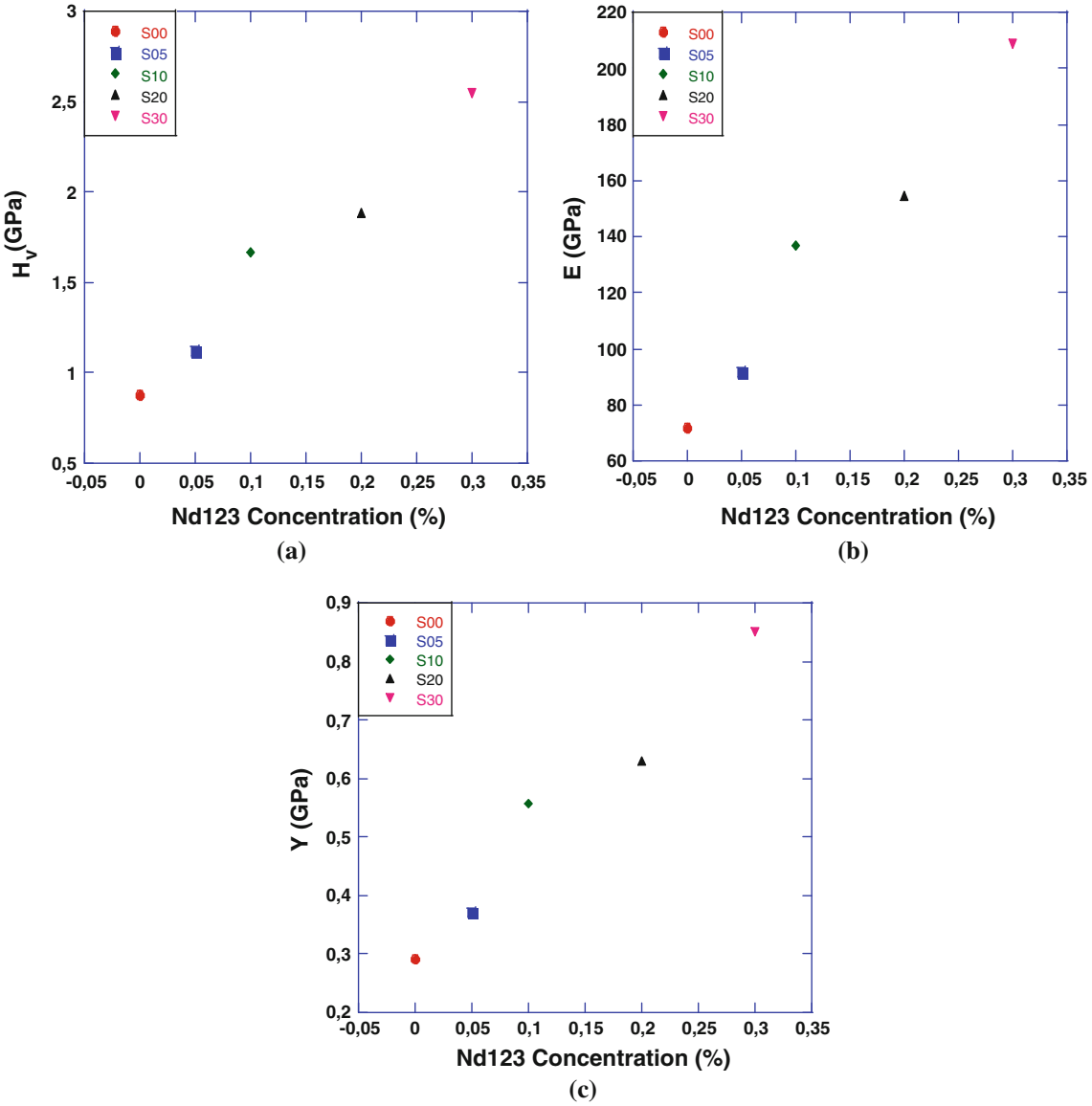

Fig. 4 Variation of load independent **a** H_v, **b** *E,* and **c** *Y* versus *Nd123*-Concentration for all samples under the load of 2.940 N

calculated grain size summarized in Table 1. As can be seen from the table, the average grain size of samples decreases with increasing Nd123 content. This is thought to be that increasing of Nd123 content increased the number of the solidification center of Sm123 from Nd123 part, and resulted in decrease in the grain size.

3.4 Vickers microhardness measurements

We have performed microhardness analyses by a digital microhardness device at room temperature in order to determine to effect of Nd123 doping on mechanical properties of S00, S05, S10, S20 and S30 samples. The applied load (F) was varied from 0.245 to 2.940 N and the indentation was suppressed 10 s at different sites of the sample surface. Optical trace indentation photographs of the samples for the load of 2.490 N are shown in Fig. 3. For each sample, five tests of indentation with each load were carried out and later the average value of the diagonal lengths of the indentation in each test was calculated. Vickers microhardness values of the samples are calculated according to the following relation

$$H_v = 1854.4(F/d^2) \quad (2)$$

where *d* is diagonal length of the indentation. In addition to elastic modulus (*E*), yield strength (*Y*) and fracture toughness (K_{IC}) parameters that are dependent on

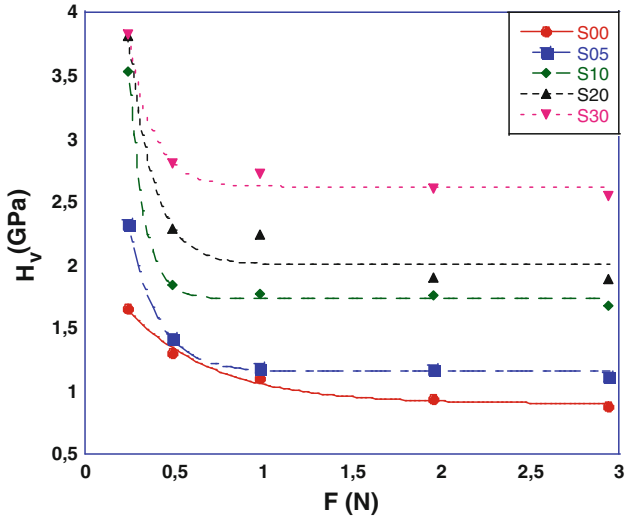

Fig. 5 Variation of load dependent microhardness H_v with applied load F

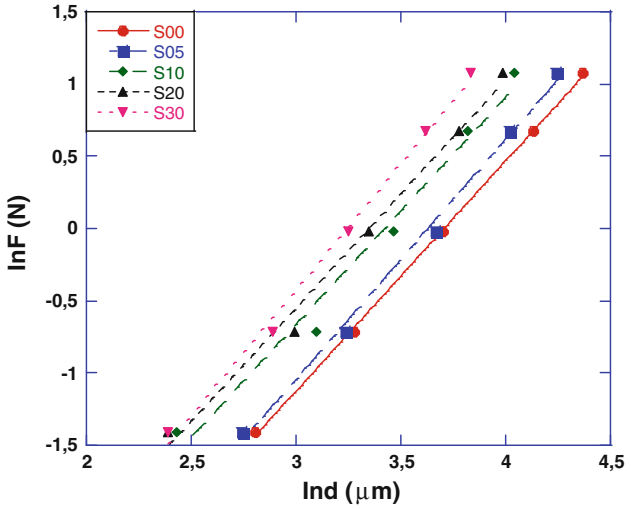

Fig. 6 Variation of applied load *lnF* with diagonal *lnd* for the samples

Table 3 Best-fit results of experimental data according to Meyer's law

Samples	n_K	lnA_{1K} (GPa)	H_V (GPa)
S00	1.59	−5.90	0.878–0.930
S05	1.66	−6.02	1.117–1.175
S10	1.56	−5.36	1.670–1.755
S20	1.57	−5.27	1.887–1.902
S30	1.74	−5.64	2.550–2.600

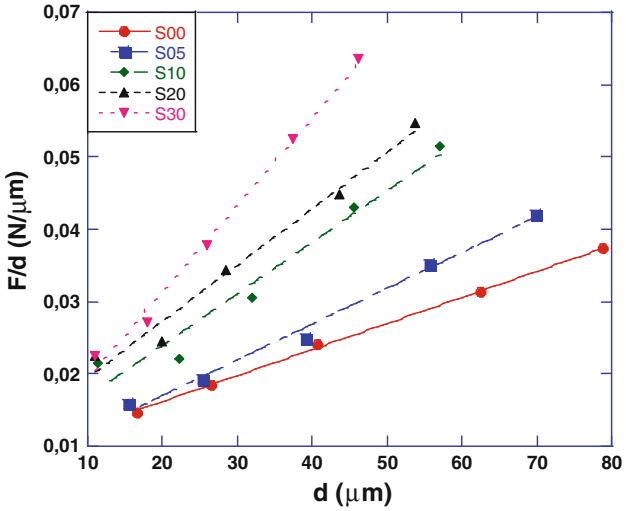

Fig. 7 Plots of *F/d* versus *d* for the samples

Table 4 Best-fit results of experimental data according to *PSR* model

Samples	$y*10^{-5}$ (N/μm)	H_{PSR} (GPa)	$x*10^{-3}$ (N/μm)	H_v (GPa)
S00	36.00	0.667	8.98	0.878–0.930
S05	49.48	0.916	7.12	1.117–1.184
S10	71.17	1.318	9.76	1.670–1.766
S20	77.80	1.442	11.74	1.887–2.235
S30	120.06	2.225	7.40	2.550–2.717

Table 5 The calculated load independent H_0, E_0, Y_0 and K_{IC} for the samples

Samples	H_0 (GPa)	E_0 (GPa)	Y_0 (GPa)	K_{ic} (Pa/$m^{1/2}$)	H_v (GPa)
S00	0.667	54.66	0.222	990.82	0.878–0.930
S05	0.916	75.07	0.305	1033.92	1.117–1.184
S10	1.318	108.02	0.439	1452.08	1.670–1.766
S20	1.442	118.19	0.480	1665.86	1.887–2.235
S30	2.225	182.36	0.741	1642.84	2.550–2.717

microhardness values of samples were calculated using the following equations.

$$E = 81.9635H_v \tag{3}$$

$$Y \approx \frac{H_v}{3} \tag{4}$$

$$K_{IC} = \sqrt{2Ex}\,(x,\ \text{surface energy}) \tag{5}$$

The calculated values are summarized in Table 2. It's noted that the values of microhardness increase with increasing the Nd123 doping. We can say that Nd123 doping helps to solidification of Sm123 to fill the intergrain of Nd123 and so microhardness values increase.

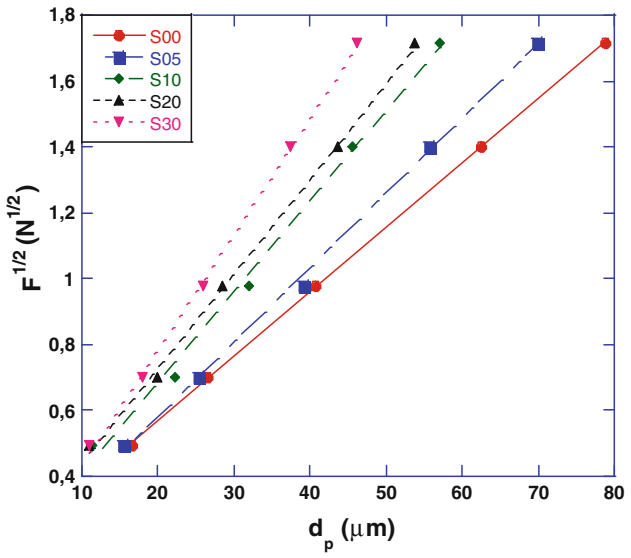

Fig. 8 Plots of square root of applied loads for the samples versus diagonal length

Table 6 Best-fit results of experimental data according to *EPD* model

Samples	A_1 (N/μm^2)	d_e (μm)	H_{EPD} (GPa)	H_V (GPa)
S00	0.019	0.178	0.669	0.878–0.930
S05	0.022	0.126	0.897	1.117–1.184
S10	0.027	0.132	1.351	1.670–1.766
S20	0.028	0.156	1.453	1.887–2.235
S30	0.034	0.089	2.143	2.550–2.717

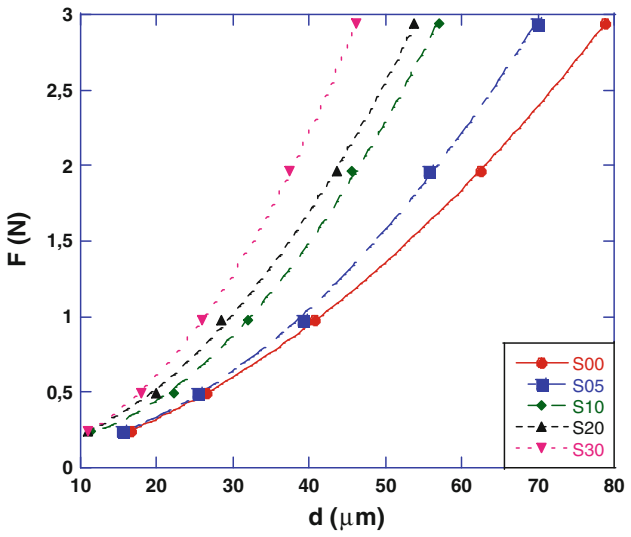

Fig. 9 Variation of applied load with the indentation diagonal length for the samples

The values of E, Y and K_{IC} of the samples are shown in Table 2. It is observed that E, Y and H_v increase monotonically with Nd123 doping (Fig. 4). The origin of increase is filling of Sm123 to the intergrains on Nd123 and resulted in increase the microhardness [5]. The detailed information on the load independent of elastic modulus, yield strength and fracture toughness can be found in reports [6–8].

The value of Vickers microhardness with the increasing of applied load, shown in Fig. 5, exponentially decreases to plateau values for all the samples. This phenomenon is known as ISE (Indentation Size Effect) [9–11]. The microhardness values decrease to the plateau value at about 1–2 N for all samples. Some factors of ISE behavior are the load required for plastic deformation, elastic recovery, the material's response to material elastic/plastic composite (mixed) deformation, the size of the trace formed during the indentation process and the combination of frictional resistance and elastic resistance of the samples.

ISE behaviors of the samples in this study were analyzed and discussed in the following by using the Meyer Law, Proportional Specimen Resistance Model (PSR), Modified Proportional Specimen Resistance Model (MPSR), Elastic/Plastic Deformation Model (EPD) and Hays–Kendall Approach.

3.5 Meyer's law

The simplest way to describe the normal ISE behavior of the materials is Meyer's law. In this method, the applied load (F) is related to indentation size (d) according to the formula.

$$F = A_{1K} d^{n_K} \tag{6}$$

where n_K and A_{1K} are calculated from the plots of InF versus Ind (Fig. 6). n is Meyer number which describes the ISE. If the value of n is less than 2, material has got the ISE behavior. If n_K is greater than 2, material has got the RISE behavior and n is equal to 2, H_v is independent of the applied load [12–15].

Typical plots of the dependence on InF of Ind for the samples are shown in Fig. 6, and analysis results of this graph according to Eq. (6) were listed in Table 3. It's clear that the values of n_K are less than 2 which confirm that our samples show the normal ISE behavior. So microhardness decreases with increasing the applied load.

3.6 PSR Model

According to several authors [16–20] have suggested that the ISE behavior may be defined by Proportional Specimen Resistance (PSR) Model whose the relation was described in Eq. (7).

Table 7 Best-fit results of experimental data according to *MPSR* model

Samples	W_{MPSR} (N)	$A_{0MPSR} \times 10^{-5}$ (N/μm)	$A_{1MPSR} \times 10^{-5}$ (N/μm^2)	H_{MPSR} (GPa)	H_V (GPa) (Plateu region)
S00	0.018	1,022.4	34.59	0.641	0.878–0.930
S05	0.076	1,810.9	56.39	1.045	1.117–1.184
S10	0.139	−308.8	92.33	1.594	1.670–1.766
S20	0.096	298.4	92.46	1.714	1.887–2.235
S30	0.075	−4.954	134.39	2.484	2.550–2.717

$$F = xd + yd^2 \quad (7)$$

$$\frac{F}{d} = x + yd \quad (8)$$

where x and y values are calculated from the plots of F/d versus d (Fig. 7). The parameter x characterizes the load dependence of hardness. The real microhardness value is proportional to y. In *PSR* model the load independent microhardness value is calculated as:

$$H_{PSR} = 1854.4y \quad (9)$$

All of x values are positive as can be seen from Table 4. This fact confirms presence of elastic deformation as well as plastic deformation in the samples studied. In addition, load independent microhardness values calculated using PSR model are given in Table 4. Moreover the calculated load dependent microhardness values (plateau region), listed in Table 2, are higher than these values [6, 21]. Therefore, it is clear that PSR model is not adequate for determination of the real microhardness value.

In addition, using load independent H_{PSR} values, load independent E, Y and K_{IC} values of the samples were calculated by Eqs. (3–5) and listed in Table 5. According to the results, the calculated load independent values are found to be lower than the load dependent values shown in Table 2. Similar behaviors in the elastic modulus, yield strength and fracture toughness are reported in the literature [22].

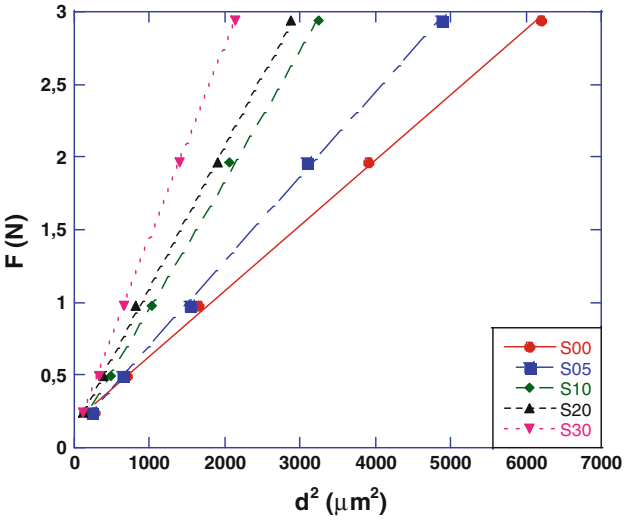

Fig. 10 Applied load versus the square of the indentation diagonal length for the samples

Table 8 Best-fit results of experimental data according to *HK* model

Samples	A_{HK} (GPa)	W_{HK} (N)	H_{HK} (GPa)	H_V (GPa)
S00	44.98×10^{-5}	0.176	0.834	0.878–0.930
S05	58.45×10^{-5}	0.108	1.083	1.117–1.184
S10	88.00×10^{-5}	0.096	1.631	1.670–1.766
S20	96.89×10^{-5}	0.135	1.796	1.887–2.235
S30	134.3×10^{-5}	0.074	2.490	2.550–2.717

3.7 EPD Model

According to Bull and et al. indenter size depend on the applied load with the relation as below [23, 24]

$$F = A_1(d_e + d_p)^2 \quad (10)$$

where A_1 is constant, d_e is related to d_p plastic deformation. The values of A_1 and d_e are calculated from $F^{1/2}$ versus d_p graph shown in Fig. 8. The load independent microhardness value is calculated from Eq. (11).

$$H_{EPD} = 1854.4A_1 \quad (11)$$

When this model is analyzed, d_e which found from the point that graph intersects the axis y is positive for all samples as seen in Table 6. When the load was applied with 10 s and then removed from the surface of sample, a small amount of elastic recovery was observed around of indenter. Elastic recovery has been observed only for the samples showing the ISE behavior [25]. The reason for the observation of indentation size effect (ISE) is the formation as well as elastic deformation. Reverse of this behavior may be possible for only the plastic deformation.

Value d_e of these materials is negative [9]. This result is observed in the samples showing the RISE (Reverse Indentation Size Effect) behavior [22]. Microhardness values of these samples increase with increasing the

Table 9 The results of load dependent Vickers microhardness at the plateau region and load independent hardness values calculated using *PSR*, *MPSR*, *EPD* and *HK* models

Samples	H_V (GPa) (in plateau region)	H_{PSR} (GPa)	H_{EPD} (GPa)	H_{MPSR} (GPa)	H_{HK} (GPa)
S00	0.878–0.930	0.667	0.669	0.641	0.834
S05	1.117–1.184	0.916	0.897	1.045	1.083
S10	1.670–1.766	1.318	1.351	1.594	1.631
S20	1.887–2.235	1.442	1.453	1.714	1.796
S30	2.550–2.717	2.225	2.143	2.484	2.490

applied load. Further, as can be seen from Table 6, EPD model is not sufficient for determination of the original microhardness value.

3.8 MPSR Model

Modified PSR model is suggested by Gong et al. [1] examining the ISE behavior in different materials. The model is given by Eq. (12).

$$F = W_{MPSR} + A_{0MPSR}d + A_{1MPSR}d^2 \quad (12)$$

According to this model, the physical meaning of A_{0MPSR} and A_{1MPSR} parameters are same as the ones in proportional sample resistance model [13]. These parameters were obtained from *F–d* graph as shown in Fig. 9. Using MPSR model, the load independent hardness values are calculated following equation:

$$H_{MPSR} = 1854.4A_{1MPSR} \quad (13)$$

The values of W_{MPSR}, A_{0MPSR}, A_{1MPSR} and load independent hardness were listed in Table 7. It's clear that, *W* values of all the samples are positive. This means that elastic and plastic deformation have been observed in all of Nd123 doped and undoped samples. Moreover, the values of load independent microhardness calculated using MPSR model are also far from the values of the plateau region. As a result, this model has been insufficient for determination the mechanical properties of the samples (Table 7).

3.9 Hays–Kendall approach

Hays and Kendall [26] researched that there is a minimum applied load W, which is essential to start plastic deformation and if this resistance is not exceed with applied load, plastic (permanent) deformation does not occur and only elastic deformation is observed. Then Hays and Kendall provided that the experimentally measured indentation size is proportional to an effective load $F_{eff} = F - W_{HK}$ instead of the applied load, *F*

$$F - W_{HK} = A_{HK}d^2 \quad (14)$$

where A_{HK} is load independent constant. Values of W_{HK} and A_{HK} were calculated by using $F–d^2$ graph (Fig. 10). For this model, the load independent hardness value were calculated using Eq. (15).

$$H_{HK} = 1854.4A_{HK} \quad (15)$$

The slope of *F* versus d^2 graph gives A_{HK} value. The values of W_{HK}, A_{HK} and load independent microhardness were listed in Table 8. As can be seen in Table 8, W_{HK} is positive. This can be explained that applied load is adequate both elastic and plastic deformation [14, 25]. Based on this conclusion, elastic and plastic deformation have been observed in all of Nd123 doped and undoped samples.

The microhardness results calculated by using the model which used in this study and the microhardness values in plateau region were listed in Table 9. The results showed that the best agreement with the values of plateau region is the results of HK approach. As described in the literature, load independent hardness value is expected to be close to the plateau region [27, 28]. Therefore, it can be concluded that the HK approach is the most successful model to explain our experimental data.

4 Conclusion

In this study, the samples in the forms of $(Sm123)_{1-x}(Nd123)_x$ for x = 0.00, 0.05, 0.10, 0.20, and 0.30 (S00, S10, S15, S20, and S30) structures were fabricated by the solid state reaction method. In the fabrication of $(Sm123)_{1-x}(Nd123)_x$ samples, the sintered Nd123 content at higher temperature than that of Sm123 was added to the calcined Sm123, mixed, and then sintered in the cylindrical pellet form. The sintering temperature of the pellets is near below the decompose temperature of Nd123 and near that of Sm123. Sm123 structure is partly in liquid form at the sintering temperature. The solidification of Sm123 is thought to start from Nd123 side and to result in decrease of grain size. Grain size decreased with increasing of Nd123 content in the sample as shown in Table 1. The solidification of Sm123 from Nd123 side makes the connection between grains. This increased the microhardness as shown in Fig. 5. The minimum load of the plateau region decreased with the increasing of Nd123 content.

This means that the smallest load for the load independent microhardness decreased with the increase of Nd123 content. In the comparison of the averaged microhardness values in plateau regions of the samples, the load independent microhardness value increased with increase Nd123 content. The difference between the microhardness value at the minimum load (0.245 N) and that of plateau region increased with the increasing of Nd123 content until $x = 0.10$, and then decreased up to $x = 0.30$.

Based on the results, the following conclusions can be summarized.

1. According to XRD analysis, lattice parameters *a* and *b* decrease linearly with increasing Nd123 doping.
2. The SEM results show that porosity decreases with increase of Nd123.
3. The average grain size of samples decreases with increasing Nd123 doping because of the increase of solidification centers. This result is confirmed by the SEM analysis.
4. Vickers microhardness values increase with increasing Nd123. This result seems to be compatible with our SEM analysis since the grain connectivity enhances and porosity decreases with increase of Nd123 content.
5. Elastic modulus, yield strength and fracture toughness values both load dependent and load independent case increase with doping.
6. The experimental results of the microhardness measurements are analyzed using Meyer's Law, PSR Model, EPD Model, MPSR Model and HK Approach.
7. The calculated load independent hardness values by HK approach are more suitable than those obtained by the PSR, EDP, MPSR models. Therefore, HK approach is the best model describing the microhardness of our samples.
8. The control of the microhardness value by using Nd123 content x in $(Sm123)_{1-x}(Nd123)_x$ superconducting structure can be useful in technological applications in superconductivity industry

Acknowledgments This work was supported by The Scientific and Technological Council of Turkey (TÜBİTAK) with project no: TBAG-110T622. The authors thank to Prof. Dr. Nazmi Turan Okumuşoğlu for his advices.

References

1. J.H. Gong, J.J. Wu, Z.D. Guan, J. Eur. Ceram. Soc. **19**, 2625–2631 (1999)
2. A.A. Elmustafa, D.S. Stone, J. Mech. Phys. Solids **51**, 357–381 (2003)
3. A. Leenders, M. Ullrich, H.C. Freyhardt, Physica C **279**, 173–180 (1997)
4. R.S. Vennila, N.V. Jaya, S. Natarajan, Mater. Lett. **59**, 1764–1766 (2005)
5. O. Ozturk, C. Terzioglu, I. Belenli, J. Supercond. Nov. Magn. **24**, 381–390 (2011)
6. M. Yilmazlar, H.A. Cetinkara, M. Nursoy, O. Ozturk, C. Terzioglu, Physica C-Supercond. Appl. **442**, 101–107 (2006)
7. U. Kolemen, O. Uzun, M. Yilmazlar, N. Guclu, E. Yanmaz, J. Alloy. Compd. **415**, 300–306 (2006)
8. H. Aydin, O. Cakiroglu, M. Nursoy, C. Terzioglu, Chin. J. Phys. **47**, 192–206 (2009)
9. R. Awad, A.I. Abou Aly, M. Kamal, M. Anas, J. Supercond. Nov. Magn. **24**, 1947–1956 (2011)
10. N.H. Mohammed, A.I. Abou-Aly, I.H. Ibrahim, R. Awad, M. Rekaby, J. Alloy. Compd. **486**, 733–737 (2009)
11. U. Kolemen, J. Alloy. Compd. **425**, 429–435 (2006)
12. E. Asikuzun, O. Ozturk, H.A. Cetinkara, G. Yildirim, A. Varilci, M. Yilmazlar, C. Terzioglu, J. Mater. Sci.-Mater. Electron. **23**, 1001–1010 (2012)
13. J.B. Quinn, G.D. Quinn, J. Mater. Sci. **32**, 4331–4346 (1997)
14. O. Ozturk, H.A. Cetinkara, E. Asikuzun, M. Akdogan, M. Yilmazlar, C. Terzioglu, J. Mater. Sci.-Mater. Electron. **22**, 1501–1508 (2011)
15. H.A. Cetinkara, M. Yilmazlar, O. Ozturk, M. Nursoy, C. Terzioglu, International conference on superconductivity and magnetism (Icsm), p. 153 (2009).
16. H. Li, R.C. Bradt, J. Mater. Sci. **28**, 917–926 (1993)
17. Q. Ma, D.R. Clarke, J. Mater. Res. **10**, 853–863 (1995)
18. F. Fröhlich, P. Grau, W. Grellmann, Phys. Stat. Sol. (a) **42**, 79–89 (1977)
19. B.D. Michels, G.H. Frischat, J. Mater. Sci. **17**, 329–334 (1982)
20. W.C. Oliver, R. Hutchings, J.B. Pethica, in *Microindentation Techniques in Materials Science and Engineering,* ed. by P.J. Blau, B.R. Lawn (ASTM, Philadelphia, PA, 1986), p. 90
21. M. Yilmazlar, O. Ozturk, O. Gorur, I. Belenli, C. Terzioglu, Supercond. Sci. Technol. **20**, 365–371 (2007)
22. K. Sangwal, Mater. Chem. Phys. **63**, 145–152 (2000)
23. G.P. Upit, S.A. Varchenya, Phys. Status Solidi B **17**, 831–835 (1966)
24. S.J. Bull, T.F. Page, E.H. Yoffe, Mag. Lett. **59**, 281–288 (1989)
25. O. Ozturk, J. Mater. Sci.: Mater. Electron. **23**, 1235–1242 (2012)
26. C. Hays, E.G. Kendall, Metallurgica **6**, 275–282 (1973)
27. J.H. Gong, Z. Zhao, Z.D. Guan, H.Z. Miao, J. Eur. Ceram. Soc. **20**, 1895–1900 (2000)
28. Z. Peng, J. Gong, H. Miao, J. Eur. Ceram. Soc. **24**, 2193–2201 (2004)